This article has been accepted for publication in IEEE/OSA Journal of Lightwave Technology. This is the author's version which has not been fully edited and content may change prior to final publication. Citation information: DOI 10.1109/JLT.2023.3265167

Analytical Formulas for Micro-Bending and Surface Scattering Loss Estimation in Tube Lattice Fibers

Federico Melli, Lorenzo Rosa, *Member, IEEE, Member, OSA,* and Luca Vincetti, *Senior Member, IEEE*

***Abstract*—Simple analytical formulas for micro-bending and surface scattering loss in Hollow-Core Tube Lattice Fibers are here proposed and numerically validated. They can also be applied to other Hollow-Core fibers with similar core-cladding interfaces such as Hybrid cladding Kagome-Tubular, Nested Tubes, and Kagome fibers. Scaling laws for both loss mechanisms are also given and discussed.**

I. Introduction

HOLLOW-Core Fibers (HCFs) represent one of the most remarkable innovations in the field of specialty optical fibers [1]. More precisely, Hollow-Core Inhibited Coupling Fibers (HC-ICFs) exhibit much better performance than Photonic Band-Gap Fibers in terms of lower loss, wider bandwidth, lower dielectric interaction, better and more flexible management of the effectively single-mode condition. Thanks to that, several applications in the fields of sensing [2], [3], optical communications [4], fiber lasers [5], high power delivery [6], [7], nonlinear optics [1], and quantum applications [8] have been demonstrated in the last few years. One of the main issues of HC-ICFs is the propagation loss (PL), which has as its lower theoretical limit the confinement loss (CL) related to the intrinsically leaky nature of their guided modes. In the last few years, a major research effort has been expended in order to reduce as much as possible the PL, mainly by acting on the CL. The deployment in succession of the core negative curvature [9], the use of tubes as microstructured cladding [10], the addition of nested tubes [11], and hybrid cladding [12] have resulted in several record low-loss designs, allowing to get closer and closer and ultimately break the limit given by silica Rayleigh scattering [4], [12]–[14]. However, experimental results show that there is a gap between the PL values and CL ones [15]–[17]. Even though a thorough theoretical analysis showing in detail the causes of this gap is not yet available, currently the additional loss is attributed to non-idealities of the real fibers and in particular to dielectric surface roughness and fiber micro-bending [4], [16], [17]. The presence of thermodynamic surface waves in the molten glass that get frozen in place upon hardening makes the dielectric-air interface rough, causing surface scattering loss (SSL) [18]. The small fiber cross-section deformations due to a non-perfect drawing process or lateral contacts of the fiber with surfaces once cabled cause further additional loss, named micro-bending loss (MBL) [19]. SSL is currently estimated by using an empirical formula [11], while MBL estimation borrows from the approaches developed in the 1980s for solid core fibers [20], [21]. SSL and MBL formulas are based on parameters which can be obtained from numerical modal solvers.

As an alternative tool to the numerical simulation, empirical analytical formulas have been proposed for the estimation of the minimum values of CL and SSL in each transmission window [22]. The CL formula has then been extended to consider also the high-loss regions caused by the coupling of the guided mode with cladding modes [23]. Analytical formulas represent an useful and effective additional tool complementary to numerical simulations, because they allow for preliminary quick design of the fibers.

In this paper, we extend this approach in order to take into account the effects of cladding mode coupling on SSL and propose an analytical formula for MBL. We also propose an improvement on the analytical formula of the effective index of HOM LP_{11} with respect to Marcatili's ones [24]. The formulas have been tested and compared with the numerical approach by considering several Tube Lattice Fibers (TLFs) with different geometrical and physical parameters, showing good accuracy. Since the formulas depend on parameters mainly affected by the core-cladding boundary, we also show that they can be effectively applied to other HC-ICFs such as hypocyclidal Kagome Fibers (KFs) [25], Nested Tube Fibers (NTFs) [11], and Hybrid cladding Kagome-Tubular Fiber (HKTFs) [12]. These formulas complete the set of analytical formulas for the estimation of the propagation loss in TLFs, which can be fruitfully applied for preliminary TLF design or analysis in conjunction with subsequent more time-consuming numerical simulations.

II. The Model

SSL is caused by the roughness of the air-dielectric interface, primarily due to the frozen-in thermal surface capillary waves excited during the fiber drawing process [18]. The estimation of SSL is complex, because it would require a statistical treatment of the scattering process, which requires an accurate knowledge of the surface roughness spectral density and of the coupling mechanisms between guided and radiating modes. Since in practice it is hard to measure such kind of quantities, and a thoroughly theoretical analysis of the coupling mechanisms is not yet available, a simplified

F. Melli and L. Vincetti are with the Department of Engineering "Enzo Ferrari", University of Modena and Reggio Emilia, I-41125 Modena, Italy e-mail: luca.vincetti@unimore.it

L. Rosa is with the Department of Engineering "Enzo Ferrari", University of Modena and Reggio Emilia, I-41125 Modena, Italy and with the Applied Plasmonics Lab, Centre for Micro-Photonics, Swinburne University of Technology, Hawthorn, VIC 3122, Australia

Manuscript received December xx, 2022; revised xxx xx, 2022.

This work is licensed under a Creative Commons Attribution 4.0 License. For more information, see https://creativecommons.org/licenses/by/4.0/

This article has been accepted for publication in IEEE/OSA Journal of Lightwave Technology. This is the author's version which has not been fully edited and content may change prior to final publication. Citation information: DOI 10.1109/JLT.2023.3265167

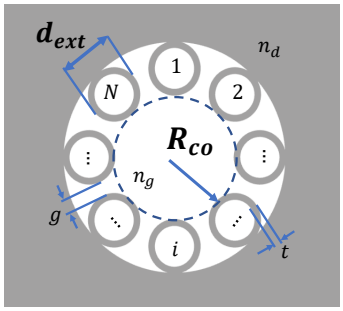

Fig. 1. TLF cross-section with geometrical and physical parameters. R_{co} core radius, d_{ext} tube external diameter, t tube thickness, g tube-tube gap, n_d dielectric refractive index (gray region), n_g refractive index of the material filling the hollow core and tubes (white region).

approach based on the following formula is currently largely used for SSL estimation [11]:

$$SSL(\lambda) = \eta \cdot EI(\lambda) \left(\frac{\lambda_0}{\lambda}\right)^3 \quad [dB/km] \tag{1}$$

where η and λ_0 are two coefficients depending on roughness, and EI is the electric field at the dielectric interface parameter [18]:

$$EI = \frac{\sqrt{\frac{\epsilon_0}{\mu_0}} \oint_{\Gamma_d} |\overline{E}|^2 \, d\Gamma}{\iint_{S_\infty} p_z \, dS}, \tag{2}$$

being Γ_d the air-dielectric interface, and $\overline{E}$ and p_z the electric field and the Poynting vector axial component of the mode, respectively. The EI parameter depends on the the wavelength and on the geometrical and physical fiber parameters shown in Fig. 1: the core radius R_{co}, the tube external diameter d_{ext}, the tube thickness t, the tube-tube gap g, the dielectric refractive index n_d and the refractive index of the material filling the hollow core and the tubes n_g. It can be calculated once the mode field distribution is obtained by using a numerical mode solver. However, its minimum value EI_{min} in each transmission band can be obtained with the following formula [22]:

$$EI_{min} = 0.63 \left(\frac{\lambda}{R_{co}}\right)^2 \frac{1}{R_{co}}. \tag{3}$$

The estimation over a wider spectral range can be done by taking into account the coupling of the FM with the cladding modes. To make the analysis more general and the graphs clearer, here we plot data as a function of normalized frequency:

$$F = \frac{2t}{\lambda}\sqrt{n_d^2 - n_g^2} \tag{4}$$

instead of the wavelength. In fact, integer values of the normalized frequency ($F = m$) correspond to the red edges of the High-Loss Regions (HLRs) irrespective of fiber's parameters [23]. At those values of F, the guided mode is phase matched with leaky cladding modes having the slowest variation along the tube perimeters and thus the strongest coupling [1], [23], [26]. The condition can be re-written as $\lambda = 2t/m\sqrt{n_d^2 - n_g^2}$ which is the resonant wavelength in the tube walls [11]. The approach is the same followed to obtain analytical formulas for CL [23], dispersion parameters, and effective area A_{eff} [27]. At frequencies approaching the high-loss regions, the coupling between the FM and the cladding modes (CLMs) increases the electric field magnitude at the boundaries, and in turn this increases the EI value. EI can be thus expressed as:

$$EI_a = A \cdot EI_{min} \cdot \sum_{\nu} \left(L(F - F^{HE}_{c_{1,\nu}}) + L(F - F^{EH}_{c_{1,\nu}}) \right) \tag{5}$$

where $A = 4.4 \cdot 10^3$, $F^{HE}_{c_{\mu,\nu}}$, and $F^{EH}_{c_{\mu,\nu}}$ are respectively the cut-off frequencies of the $HE_{\mu,\nu}$ and $EH_{\mu,\nu}$ CLMs with azimuthal and radial indices μ and ν, respectively. $L(F)$ is a Lorentzian function:

$$L(F) = \frac{\gamma^2}{\gamma^2 + F^2} \tag{6}$$

with $\gamma = 3.5 \cdot 10^{-3}$. Only the coupling with CLMs having azimuthal index $\mu = 1$ is here considered, because they give the strongest coupling with the FM [27].

MBL is caused by a random tilting of the fiber longitudinal axis due to the fabrication process and/or external mechanical stress. Such fiber perturbations cause additional coupling of the FM with leaky and radiating modes, with a consequent PL enhancement of the former. In a single-mode fiber with a FM having a Gaussian field profile, the upper limit of the MBL can be estimated as [21]:

$$MBL = \frac{1}{4}\left(\frac{2\pi}{\lambda} n_{eff}^{FM}\right)^2 R_0^2 \Phi\left(\Delta\beta\right) \quad [dB/km] \tag{7}$$

with n_{eff} being the FM effective index, R_0 the FM field radius, $\Delta\beta$ the phase constant difference between FM and LP_{11} HOMs, and Φ the power spectral density (PSD) of the stochastic process describing the micro-bending.

Recently, analytical formulas for the FM effective index n_{eff} and effective area A_{eff} have been proposed [27]. The effective index formula is based on Marcatili's one [24], but with an additional term Δn_{eff} and an equivalent radius $R_{co_{eff}}$:

$$n_{eff}^{FM} = n_g - \frac{1}{2}\left(\frac{u_{0,1} 2t\sqrt{n_d^2 - n_g^2}}{2\pi R_{co_{eff}} F \sqrt{n_g}}\right)^2 + \Delta n_{eff}(F), \tag{8}$$

being $u_{0,1}$ the first zero of the Bessel function of order zero, and n_g the refractive index of the material filling the core and the tubes. Δn_{eff} takes into account the anti-crossing caused by coupling with cladding modes and $R_{co_{eff}}$ accounts for the hypocycloidal shape of the core-cladding interface. The effective area formula is based on the observation that the effective area is a function of the effective index [27]:

$$A_{eff} = \frac{0.48}{8\pi} \frac{(u_{0,1}\lambda)^2}{n_g(n_g - n_{eff}^{FM})}. \tag{9}$$

Finally, in the context of the Gaussian approximation of the FM field profile [28]:

$$R_0^2 = \frac{A_{eff}}{\pi}, \tag{10}$$

By substituting Eq. (9) in Eq. (10), the latter in Eq. (7), and multiplying it by a factor $0.9025\sqrt{(N - 0.68)/(N - 1)}$ dependent on the number of tubes N surrounding the core,

This work is licensed under a Creative Commons Attribution 4.0 License. For more information, see https://creativecommons.org/licenses/by/4.0/

This article has been accepted for publication in IEEE/OSA Journal of Lightwave Technology. This is the author's version which has not been fully edited and content may change prior to final publication. Citation information: DOI 10.1109/JLT.2023.3265167

TABLE I
TLF PARAMETERS
ALL GEOMETRICAL PARAMETERS ARE GIVEN IN MICROMETERS

Fiber	t	d_{ext}	n_d	N	g	R_{co}
#1	0.50	20.0	1.45	8	2.96	20.00
#2	0.50	14.0	1.45	8	2.96	15.16
#3	0.50	14.0	1.45	6	2.97	9.97
#4	0.50	14.0	1.45	5	2.96	7.43
#5	0.50	24.0	1.45	8	5.08	26.00
#6	0.50	14.0	2.45	8	2.96	15.16

which has been introduced in order to take into account the hypocycloidal shape of the core-cladding interface, it results:

$$MBL_a = 5.415{\cdot}10^{-2}\sqrt{\frac{N-0.68}{N-1}}u_{0,1}^2\frac{(n_{eff}^{FM})^2}{n_g(n_g-n_{eff}^{FM})}\Phi(\Delta\beta). \tag{11}$$

The last element required for having a complete analytical expression of MBL is the phase constant difference $\Delta\beta$ between the FM LP_{01} and the HOM LP_{11}. Here we propose to extend Eq. (8) according to Marcatili's formula, that is by replacing $u_{0,1}$ with the first root of the first-order Bessel function $u_{1,1}$:

$$n_{eff}^{HOM} = n_g - \frac{1}{2}\left(\frac{u_{1,1}2t\sqrt{n_d^2-n_g^2}}{2\pi R_{co_{eff}}F\sqrt{n_g}}\right)^2 + \Delta n_{eff}(F) \tag{12}$$

so that

$$\begin{aligned}\Delta\beta &= \frac{2}{\pi\lambda}\left(n_{eff}^{FM}-n_{eff}^{HOM}\right)\\ &= \frac{t}{2\pi R_{co_{eff}}^2}\sqrt{\frac{n_d^2-n_g^2}{n_g^2}}\frac{u_{0,1}^2-u_{1,1}^2}{F}.\end{aligned} \tag{13}$$

Eq. (11), together with Eqs. (8), and (13), and the mathematical expression of $\Phi(\Delta\beta)$, permits to analytically estimate the MBL.

III. NUMERICAL VALIDATION

In order to validate the proposed formulas, several TLFs with different geometrical and physical parameters have been considered. Fibers' names and parameters are reported in Tab. I. Since the main approximation the approach is the Gaussian profile of the FM, fibers with different core size and shape have been considered. The core size and the hypocycloidal-like shape have been changed, both changing the tube size (fibers #1, #2, and #5) and thus their curvature, and the tube number (fibers #2, #3, and #4). Finally, by comparing fibers #2 and #6 we investigated the effect of the dielectric refractive index. Concerning SSL, Fig. 2 compares Eq. (2) calculated numerically through a modal solver, and the proposed Eq. (5). To estimate the accuracy, an error figure e_{EI} is also plotted. Due to the large range of variation of the EI parameter (at least three order of magnitude in the fibers and spectral ranges here considered), the error figure is defined as:

$$e_{EI} = \frac{EI_a}{EI}. \tag{14}$$

Black bars show the High-Loss Regions (HLRs) where PL is extremely high due to the coupling of the FM with cladding modes [26], [27]. We focus the accuracy estimation on the Transmission Bands (TBs) bounded by the HLRs. The first TB shows the worst accuracy, which is always bounded between $3/2$ and $2/3$. By excluding the first TB, the error is bounded between $\pm 20\%$.

For a fair estimation of the accuracy of the MBL formula irrespective to the chosen PSD for describing the statistics, Fig. 3 compares MBL/Φ obtained from Eqs. (7) and (11). In this case, the parameters' range of variation is narrower, so the following error figure is here used to assess the accuracy:

$$e_{MBL} = \frac{MBL - MBL_a}{MBL}. \tag{15}$$

The accuracy is pretty good, being bounded between $\pm 2\%$ in all TBs. As expected, the worst accuracy is obtained for fiber #4. The small core size combined with just five tubes makes the hypocycloidal shape of the FM field profile more pronounced, and thus the Gaussian approximation coarser. The lower the number of the tubes and the normalized frequency, the worse the Gaussian approximation the proposed formula is based on. Even though not shown in the figure, e_{MBL} is lower than 12.5% in the first TB of fiber #4.

Finally, Fig. 4 compares Eqs. (8) and (12) with the numerical results and also shows the corresponding error figures defined as

$$e_n = \frac{n_{eff_{num}} - n_{eff_{an}}}{1 - n_{eff_{num}}}. \tag{16}$$

This error figure takes into account that, by increasing the normalized frequency, the effective indices tend asymptotically to 1, so that analytical and numerical values must coincide over a higher and higher number of digits. Once again, the accuracy is pretty good and always bounded between $\pm 2.5\%$, except for fiber #4 where the analytical formulas tend to overestimate the effective indices, increasing the error which is however lower than 10%.

Finally, Fig. 5 shows a global view of the several loss components, numerically and analytically computed for fiber #1, by assuming $\Phi(\Delta\beta) = 8.0/\Delta\beta^2$. The agreement is pretty good, both for the single components (CL, SSL, MBL) and for the total loss $TL = CL + SSL + MBL$.

IV. OTHER NEGATIVE CURVATURE HC-ICFS

The formula accuracy assessment has been finally extended to other very common HC-ICFs with hypocycloidal or negative-curvature core-cladding boundary: Hybrid cladding Kagome-Tubular Fiber (HKTF), nested tube fibers (NTFs), and Kagome fiber (KF). The results obtained for these fibers are shown in Fig. 6. The geometrical parameters are the following: $R_{co} = 22.7\,\mu m$, $d_{ext} = 35.8\,\mu m$ and $t = 1.0\,\mu m$ for HKTF, and $R_{co} = 22.7\,\mu m$, $d_{ext} = 20\,\mu m$, and $t = 1.0\,\mu m$ for NTF. The dielectric refractive index is $n_d = 1.45$ for all fibers considered in this section. Since the accuracy of the model mainly depends on size and shape of the core, results are coherent with the TLFs ones. Finally, the hypocycloidal core-cladding boundary of the KF can be modeled as

This work is licensed under a Creative Commons Attribution 4.0 License. For more information, see https://creativecommons.org/licenses/by/4.0/

This article has been accepted for publication in IEEE/OSA Journal of Lightwave Technology. This is the author's version which has not been fully edited and content may change prior to final publication. Citation information: DOI 10.1109/JLT.2023.3265167

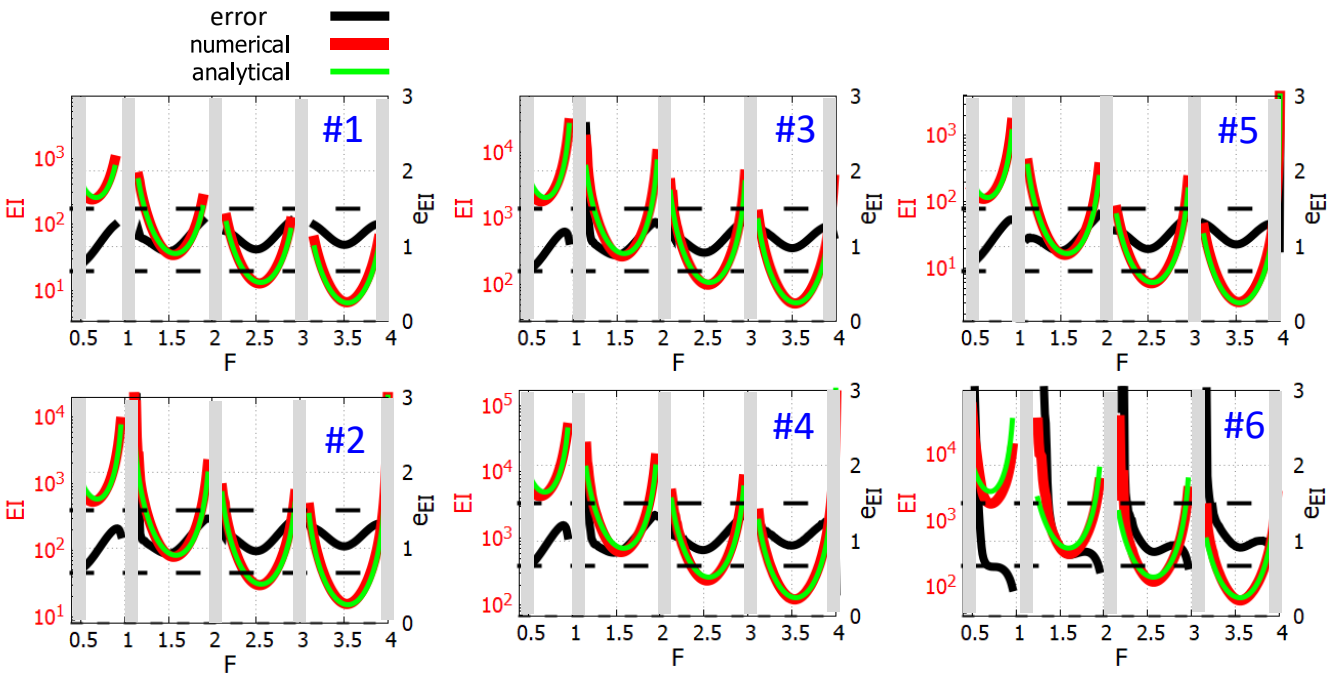

Fig. 2. EI of the six TLFs described in Tab. I. Dark regions correspond to FM high-loss spectral regions. Solid green, red, and black curves show numerical and analytical result, and relative error, respectively. Dashed horizontal lines correspond to the values $e_{EI} = 3/2$ (top) and $e_{EI} = 2/3$ (bottom).

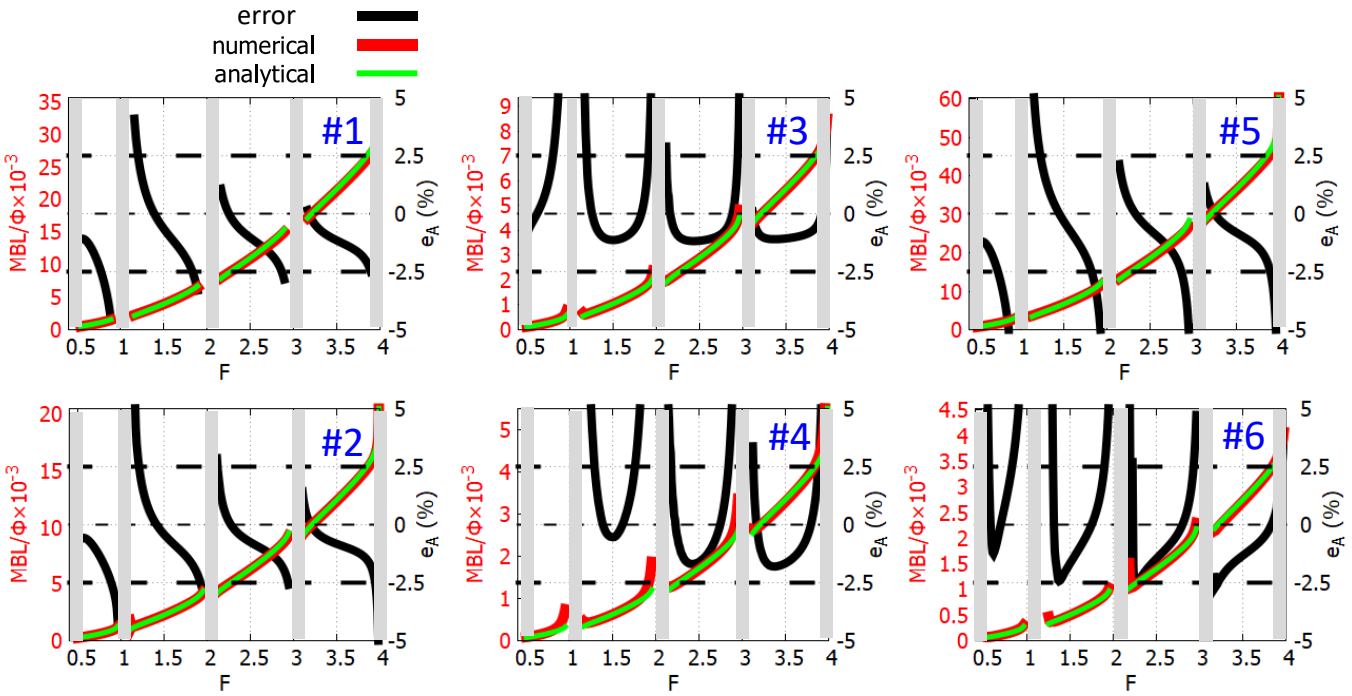

Fig. 3. MBL/Φ of the six TLFs described in Tab. I. Dark regions correspond to FM high-loss spectral regions. Solid green, red, and black curves show numerical and analytical result, and relative error, respectively. Dashed horizontal lines correspond to the values $e_{MBL} = 2.5\%$ (top) and $e_{MBL} = -2.5\%$ (bottom).

an equivalent six-tubes TLF with tubes highlighted by the red dashed circles in Fig. 7 [27]. The radius of the six tubes has been chosen equal to the radius of the largest arcs of the core-cladding contour. The used geometrical parameters are the following: $R_{co} = 22.7\,\mu m$, $d_{ext} = 19.5\,\mu m$, and $t = 1.0\,\mu m$. Despite the approximation in the contour, the accuracy of the model is consistent with the previous results, showing that the formulas can be applied also to this kind of HC-ICFs. The results reported in this and the previous section show the effects of SSL and MBL are mainly set by the size

This work is licensed under a Creative Commons Attribution 4.0 License. For more information, see https://creativecommons.org/licenses/by/4.0/

This article has been accepted for publication in IEEE/OSA Journal of Lightwave Technology. This is the author's version which has not been fully edited and content may change prior to final publication. Citation information: DOI 10.1109/JLT.2023.3265167

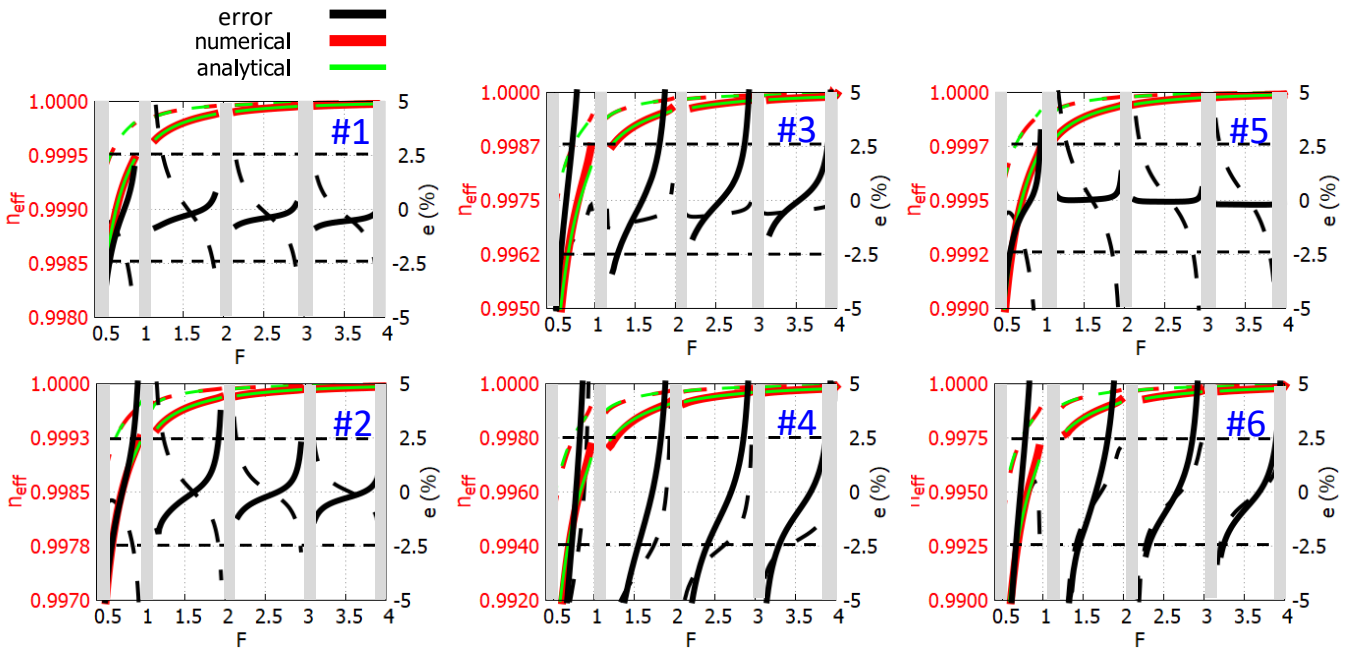

Fig. 4. Effective indices n_{eff}^{FM}, n_{eff}^{HOM} of the six TLFs described in Tab. I. Dark regions correspond to FM high-loss spectral regions. For n_{eff}^{FM}, dashed green, red, and black curves show numerical and analytical result, and relative error, respectively. For n_{eff}^{HOM}, solid green, red, and black curves show numerical and analytical result, and relative error, respectively. Dashed horizontal lines correspond to the values $e_n = 2.5\%$ (top) and $e_n = -2.5\%$ (bottom).

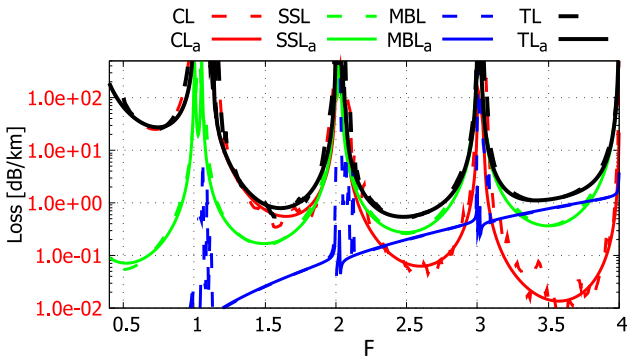

Fig. 5. Single loss terms, CL (red), SSL (green), MBL (blue) and total loss TL (black), numerically (dashed lines) and analytically (solid lines) computed for the fiber $\#1$ by setting $\eta = 300 \cdot 10^{-6}$, $\lambda_0 = 1700\,nm$, and $\Phi = 8.0/\Delta\beta^2$.

and the shape of the core. The cladding structure outside the core-cladding interface (nested tubes, kagome lattice), which greatly affect the confinement loss, have negligible effects on SSL and MBL.

V. Scaling Laws

Another advantage of having analytical formulas is the possibility to obtain useful scaling laws. SSL and MBL exhibit different wavelength dependence and inverse core size dependence. As a consequence, for certain combinations of geometrical parameters and working wavelengths SSL dominates MBL, and viceversa for certain others.

About SSL, by substituting Eq. (3) in Eq. (1) it results:

$$SSL_{min}(\lambda) = 0.63\eta\lambda_0^3 \frac{1}{R_{co}^3}\frac{1}{\lambda} \tag{17}$$

showing that the dependence of the minimum value SSL_{min} in each transmission band is inversely proportional to the wavelength and to the cube of the core radius. A similar formula can be obtained for MBL. In this case the relationships also depend on the PSD of the stochastic process. Despite the fact that in literature direct measurements of MBL PSD are not yet available, often the following expression is used:

$$\Phi(\Delta\beta) = \frac{C_0}{\Delta\beta^p}. \tag{18}$$

In [16], [19], Eq. 18 with $p = 2$ has been assumed. By substituting Eq. (13), and (18) into (11), it results:

$$MBL_{min} = K\frac{2^{3+2p}\pi^{2+p}}{(u_{1,1}^2 - u_{0,1}^2)^p} n_{eff}^{FM\,2} n_g^p C_0 \frac{R_{co_{eff}}^{2(p+1)}}{\lambda^{2+p}}, \tag{19}$$

with $K = 5.415 \cdot 10^{-2}\sqrt{(N-0.68)/(N-1)}$. Eq. (19) gives the dependence of the MBL at the center of each TBs on core radius and wavelength. By considering the case $p = 2$, the wavelength dependence is stronger than for the SSL, being in the present case inversely proportional to the fourth power of λ. The core radius dependence is the inverse of the SSL one. MBL increases with the core size, with a strong dependence equal to R_{co}^6 in case of $p = 2$.

Finally, by neglecting the relatively weak dependencies of MBL_{min} on N and n_{eff}^{FM}, it results:

$$\frac{MBL_{min}}{SSL_{min}} = 8.6 \cdot 10^{-2}\frac{2^{3+2p}\pi^{2+p}}{\lambda_0^3(u_{1,1}^2 - u_{0,1}^2)^p}\frac{C_0}{\eta}\frac{R_{co}^{2p+5}}{\lambda^{p+1}}. \tag{20}$$

This work is licensed under a Creative Commons Attribution 4.0 License. For more information, see https://creativecommons.org/licenses/by/4.0/

This article has been accepted for publication in IEEE/OSA Journal of Lightwave Technology. This is the author's version which has not been fully edited and content may change prior to final publication. Citation information: DOI 10.1109/JLT.2023.3265167

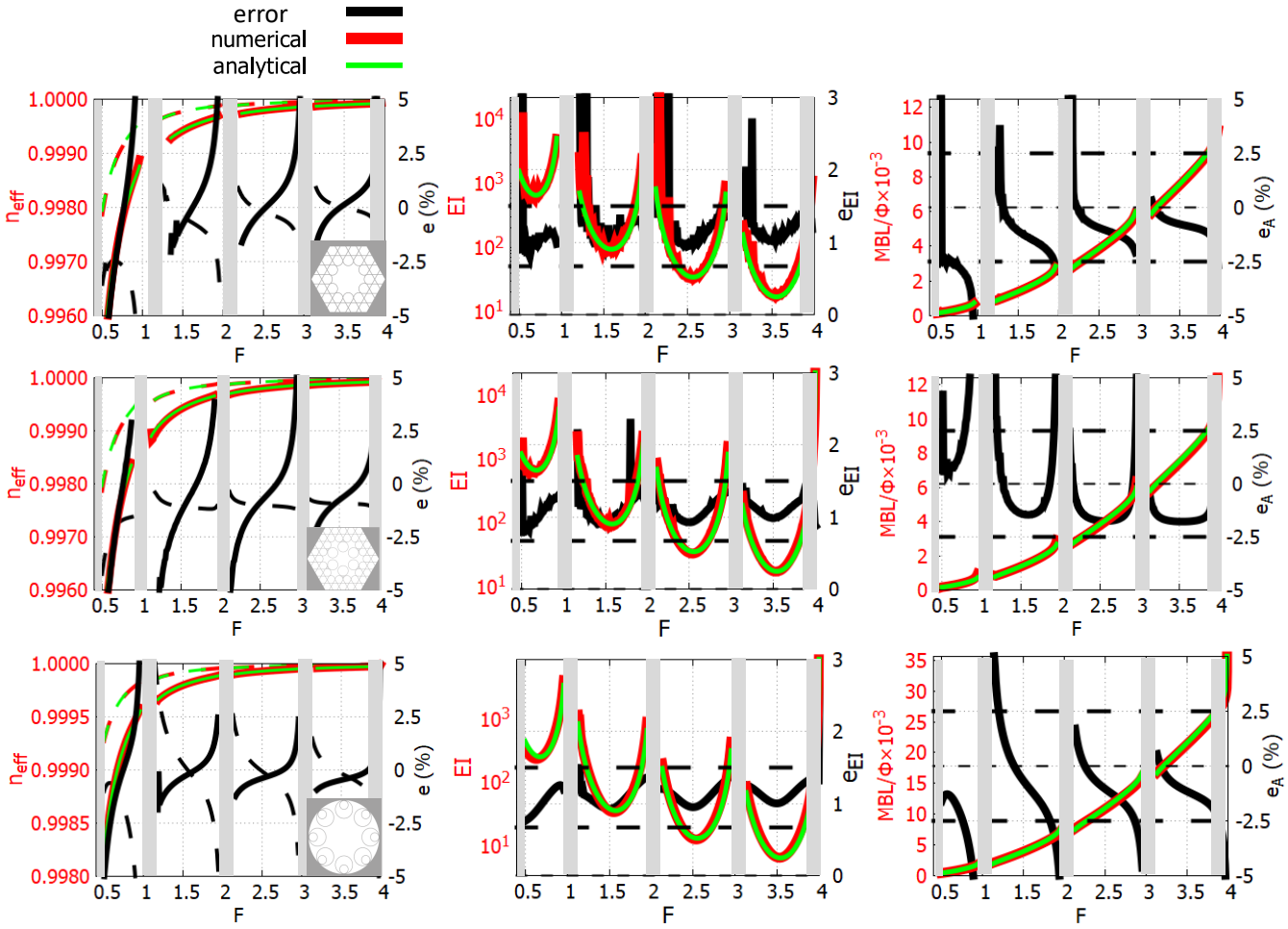

Fig. 6. From left to right: Effective indices n_{eff}^{FM}, n_{eff}^{HOM}, EI, and MBL/Φ of KF (upper line), HKTF (central line) and NTF (bottom line). with parameters: Dark regions correspond to FM high-loss spectral regions. Solid green, red, and black curves show numerical and analytical result, and relative error, respectively.

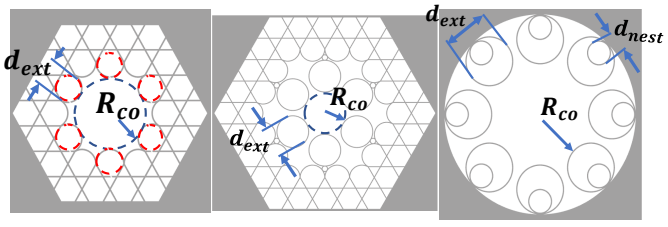

Fig. 7. From left to right: cross-sections of KF (with equivalent tubes represented by the red dashed circles), HKTF and NTF, with parameters: $R_{co} = 22.7\,\mu m$, $d_{ext} = 19.5\,\mu m$, $t = 1.0\,\mu m$, and $n_d = 1.45$ (KF), $R_{co} = 22.7\,\mu m$, $d_{ext} = 35.8\,\mu m$, $t = 1.0\,\mu m$, $n_d = 1.45$ (HKTF), $R_{co} = 20\,\mu m$, $d_{ext} = 2d_{nest} = 20\,\mu m$, $t = 0.5\,\mu m$, and $n_d = 1.45$ (NTF).

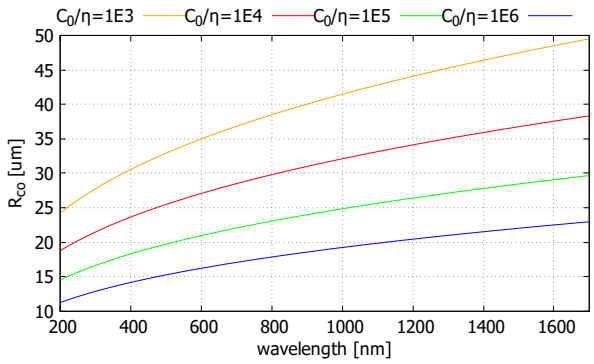

Fig. 8. (R_{co}, λ) pairs corresponding to $MBL = SSL$ for different C_0/η ratios and $p = 2$. Above the curves, MBL is greater than SSL, conversely, below them SSL dominates on MBL.

This equation shows how the ratio of the two loss sources strongly depends on the core size and, though more weakly, on the wavelength. Just as an example, Fig. 8 shows the pairs (R_{co}, λ) corresponding to $MBL_{min} = SSL_{min}$ for different values of the ratio C_0/η in case of $p = 2$. In this case, MBL_{min}/SSL_{min} scales as R_{co}^9/λ^3. MBL dominates SSL for short wavelengths and large core radii. With $C_0/\eta = 10^4$, a core radius of $24\,\mu m$ is required to have $MBL_{min} = SSL_{min}$ at $\lambda = 400nm$. The core radius can increase to $32\,\mu m$ at $1064\,nm$ and to $37\,\mu m$ at $1550\,nm$ when setting the same condition.

This work is licensed under a Creative Commons Attribution 4.0 License. For more information, see https://creativecommons.org/licenses/by/4.0/

This article has been accepted for publication in IEEE/OSA Journal of Lightwave Technology. This is the author's version which has not been fully edited and content may change prior to final publication. Citation information: DOI 10.1109/JLT.2023.3265167

VI. Conclusion

In this paper, simple analytical formulas for the estimation of surface scattering loss and micro-bending loss in Hollow-Core Tube Lattice Fibers have been proposed and numerically validated by considering several TLFs with different geometrical and physical parameters. The accuracy of the formulas is pretty good for all fibers here considered. The MBL formula is based on the Gaussian approximation of the FM field profile, consequently it is less accurate for TLFs with few tubes, where the actual FM profile differs the most from the Gaussian one. These formulas complete the set of analytical formulas allowing to estimate all the loss mechanisms defining the total loss in TLFs so far identified by the scientific community: confinement loss, surface scattering loss, and micro-bending loss. Together with the dispersion formulas both for FM LP_{01} and HOM LP_{11}, they form a useful set of equations for quick design or analysis of TLFs. All these formulas, with the exception of the CL one, can be also applied to other hollow-core inhibited-coupling fibers with a hypocycloidal (negative curvature) core-cladding interface, such as KFs, NTFs, and HKTFs, because they mainly depend on the shape and size of the hollow core. On the contrary, CL also strongly depends on the features of the microstructured cladding outside the core-cladding boundary. The CL analytical formulas currently available can only be applied to TLFs. Formulas for the estimation of CL in KFs, NTFs, and HKTFs are not yet available and will be object of future investigations.

Acknowledgments

This work is supported by the University of Modena and Reggio Emilia FAR DIP 2021 project SOQUANTS, Grant No. 554.2022, and H2020-FETOPEN-2018-2020 project CRYST^3, Grant No. 964531. F.M. acknowledges the European Commission for support through a grant in the context of H2020 project CRYST^3.

References

[1] B. Debord, F. Amrani, L. Vincetti, F. Gérôme, and F. Benabid, "Hollow-core fiber technology: The rising of "gas photonics"," *Fibers*, vol. 7, no. 2, 2019.

[2] F. Khozeymeh, F. Melli, S. Capodaglio, R. Corradini, F. Benabid, L. Vincetti, and A. Cucinotta, "Hollow-core fiber-based biosensor: A platform for lab-in-fiber optical biosensors for DNA detection," *Sensors*, vol. 22, no. 14, 2022.

[3] M. Nikodem, G. Gomółka, M. Klimczak, D. Pysz, and R. Buczyński, "Demonstration of mid-infrared gas sensing using an anti-resonant hollow core fiber and a quantum cascade laser," *Opt. Express*, vol. 27, no. 25, pp. 36 350–36 357, Dec 2019.

[4] G. Jasion, H. Sakr, J. Hayes, S. Sandoghchi, L. Hooper, E. Numkam Fokoua, A. Saljoghei, H. Mulvad, M. Alonso, A. Taranta, T. Bradley, I. A. Davidson, Y. Chen, D. Richardson, and F. Poletti, "0.174 dB/km hollow core double nested antiresonant nodeless fiber (DNANF)," in *2022 Optical Fiber Communications Conference and Exhibition (OFC)*, 2022, pp. 1–3.

[5] F. B. A. Aghbolagh, V. Nampoothiri, B. Debord, F. Gerome, L. Vincetti, F. Benabid, and W. Rudolph, "Mid IR hollow core fiber gas laser emitting at 4.6 μm," *Opt. Lett.*, vol. 44, no. 2, pp. 383–386, Jan 2019.

[6] M. Michieletto, J. K. Lyngsø, C. Jakobsen, J. Lægsgaard, O. Bang, and T. T. Alkeskjold, "Hollow-core fibers for high power pulse delivery," *Opt. Express*, vol. 24, no. 7, pp. 7103–7119, Apr 2016.

[7] "Hollow-core photonic crystal fibers for Power-over-Fiber systems," *Optical Fiber Technology*, vol. 73, p. 103041, 2022.

[8] X. Chen, W. Ding, Y.-Y. Wang, S.-F. Gao, F. Xu, H. Xu, Y.-F. Hong, Y.-Z. Sun, P. Wang, Y.-Q. Lu, and L. Zhang, "High-fidelity, low-latency polarization quantum state transmissions over a hollow-core conjoined-tube fiber at around 800 nm," *Photon. Res.*, vol. 9, no. 4, pp. 460–470, Apr 2021.

[9] Y. Y. Wang, N. V. Wheeler, F. Couny, P. J. Roberts, and F. Benabid, "Low loss broadband transmission in hypocycloid-core Kagome hollow-core photonic crystal fiber," *Opt. Lett.*, vol. 36, no. 5, pp. 669–671, Mar 2011.

[10] A. D. Pryamikov, A. S. Biriukov, A. F. Kosolapov, V. G. Plotnichenko, S. L. Semjonov, and E. M. Dianov, "Demonstration of a waveguide regime for a silica hollow-core microstructured optical fiber with a negative curvature of the core boundary in the spectral region > 3.5 μm," *Opt. Express*, vol. 19, no. 2, pp. 1441–1448, Jan 2011.

[11] F. Poletti, "Nested antiresonant nodeless hollow core fiber," *Opt. Express*, vol. 22, no. 20, pp. 23 807–23 828, Oct 2014.

[12] F. Amrani, J. H. Osório, F. Delahaye, F. Giovanardi, L. Vincetti, B. Debord, F. Gérôme, and F. Benabid, "Low-loss single-mode hybrid-lattice hollow-core photonic-crystal fibre," *Light Sci. Appl.*, vol. 10, no. 1, p. 7, Jan 2021.

[13] S.-f. Gao, Y.-y. Wang, W. Ding, Y.-f. Hong, and P. Wang, "Conquering the Rayleigh scattering limit of silica glass fiber at visible wavelengths with a hollow-core fiber approach," *Laser & Photonics Reviews*, vol. 14, no. 1, p. 1900241, 2020.

[14] G. T. Jasion, T. D. Bradley, K. Harrington, H. Sakr, Y. Chen, E. N. Fokoua, I. A. Davidson, A. Taranta, J. R. Hayes, D. J. Richardson, and F. Poletti, "Hollow core nanf with 0.28 db/km attenuation in the c and l bands," in *Optical Fiber Communication Conference Postdeadline Papers 2020*. Optica Publishing Group, 2020, p. Th4B.4.

[15] B. Debord, A. Amsanpally, M. Chafer, A. Baz, M. Maurel, J. M. Blondy, E. Hugonnot, F. Scol, L. Vincetti, F. Gérôme, and F. Benabid, "Ultralow transmission loss in inhibited-coupling guiding hollow fibers," *Optica*, vol. 4, no. 2, pp. 209–217, Feb 2017.

[16] W. Ding, Y.-Y. Wang, S.-F. Gao, M.-L. Wang, and P. Wang, "Recent progress in low-loss hollow-core anti-resonant fibers and their applications," *IEEE Journal of Selected Topics in Quantum Electronics*, vol. 26, no. 4, pp. 1–12, 2020.

[17] G. T. Jasion, T. Bradley, H. Sakr, J. R. Hayes, Y. Chen, A. Taranta, H. C. Mulvad, I. A. Davidson, N. V. Wheeler, E. N. Fokoua, W. Wang, D. J. Richardson, and F. Poletti, "Recent breakthroughs in hollow core fiber technology," in *Next-Generation Optical Communication: Components, Sub-Systems, and Systems IX*, G. Li and X. Zhou, Eds., vol. 11309, International Society for Optics and Photonics. SPIE, 2020, p. 1130902.

[18] P. J. Roberts, F. Couny, H. Sabert, B. J. Mangan, D. P. Williams, L. Farr, M. W. Mason, A. Tomlinson, T. A. Birks, J. C. Knight, and P. S. Russell, "Ultimate low loss of hollow-core photonic crystal fibres," *Opt. Express*, vol. 13, no. 1, pp. 236–244, Jan 2005.

[19] E. Numkam Fokoua, Y. Chen, D. J. Richardson, and F. Poletti, "Microbending effects in hollow-core photonic bandgap fibers," in *ECOC 2016; 42nd European Conference on Optical Communication*, 2016, pp. 1–3.

[20] H. Taylor, "Bending effects in optical fibers," *Journal of Lightwave Technology*, vol. 2, no. 5, pp. 617–628, 1984.

[21] K. Petermann and R. Kuhne, "Upper and lower limits for the microbending loss in arbitrary single-mode fibers," *Journal of Lightwave Technology*, vol. 4, no. 1, pp. 2–7, 1986.

[22] L. Vincetti, "Empirical formulas for calculating loss in hollow core tube lattice fibers," *Opt. Express*, vol. 24, no. 10, pp. 10 313–10 325, May 2016.

[23] L. Vincetti and L. Rosa, "A simple analytical model for confinement loss estimation in hollow-core tube lattice fibers," *Opt. Express*, vol. 27, no. 4, pp. 5230–5237, Feb 2019.

[24] E. A. J. Marcatili and R. A. Schmeltzer, "Hollow metallic and dielectric waveguides for long distance optical transmission and lasers," *Bell Syst. Tech. J.*, vol. 43, no. 4, pp. 1783–1809, 1964.

[25] B. Debord, M. Alharbi, T. Bradley, C. Fourcade-Dutin, Y. Wang, L. Vincetti, F. Gérôme, and F. Benabid, "Hypocycloid-shaped hollow-core photonic crystal fiber part I: arc curvature effect on confinement loss," *Opt. Express*, vol. 21, no. 23, pp. 28 597–28 608, Nov 2013.

[26] L. Vincetti and V. Setti, "Waveguiding mechanism in tube lattice fibers," *Opt. Express*, vol. 18, no. 22, pp. 23 133–23 146, Oct 2010.

[27] L. Rosa, F. Melli, and L. Vincetti, "Analytical formulas for dispersion and effective area in hollow-core tube lattice fibers," *Fibers*, vol. 9, no. 10, 2021.

[28] N. A. Mortensen, "Effective area of photonic crystal fibers," *Opt. Express*, vol. 10, no. 7, pp. 341–348, Apr 2002.

This work is licensed under a Creative Commons Attribution 4.0 License. For more information, see https://creativecommons.org/licenses/by/4.0/